BENCHMARK OF TURBULENCE MODELINGS IN A TAYLOR-COUETTE-POISEUILLE SYSTEM

Christophe Friess, Sébastien Poncet, Stéphane Viazzo

BENCHMARK OF TURBULENCE MODELINGS IN A TAYLOR-COUETTE-POISEUILLE SYSTEM

C. Friess, S. Poncet and S. Viazzo

Aix-Marseille Université, Laboratoire M2P2 UMR 7340, Marseille (France)

christophe.friess@l3m.univ-mrs.fr

1 Introduction

The present investigation is concerned with the numerical modeling of the turbulent flow in a narrow gap Taylor-Couette-Poiseuille (TCP) system. The flow is confined between two coaxial cylinders of length h, with an inner rotating cylinder (radius R_1) and a outer stationary one (radius R_2). An axial thoughflow of fluid is supplied within the gap. Such turbulent flows have many applications in process engineering (dynamic membrane filtration) and also in the turbomachinery industry (rotating heat exchangers).

The effect of an axial throughflow in a Taylor-Couette system has been considered experimentally by Kaye and Elgar (1958), who showed the existence of four flow regimes depending on the incoming flow velocity W_m and on the rotation rate Ω: laminar and turbulent flows, with or without Taylor vortices. Most of the experimental works so far have been performed in systems characterized by a high aspect ratio $\Gamma = h/\Delta R > 50$ ($\Delta R = R_2 - R_1$) and a moderate radius ratio $0.33 < \eta = R_1/R_2 < 0.66$. Thus, Nouri and Whitelaw (1994) then Escudier and Gouldson (1995) provided very useful velocity measurements for ($\Gamma = 98$, $\eta = 0.496$) and ($\Gamma = 244$, $\eta = 0.506$) respectively.

Naser (1997) compared the predictions of a $k - \varepsilon$ model with the experimental data of Escudier and Gouldson (1995). The model showed large discrepancies for the mean velocity components, with a strong dependence on the axial position not observed in the experiments. Kuosa et $al.$ (2004) performed a numerical benchmark in a Taylor-Couette system with a radial inlet. None of the two-equation models offer satisfactory results even for the mean tangential fluid velocity. Chung and Sung (2005) performed Large Eddy Simulation (LES) using second-order spatial schemes. They compared their numerical data to the experimental ones of Nouri and Whitelaw (1994) for $\eta = 0.5$ and three values of the rotation parameter $N = \Omega R_1/W_m = [0.2145; 0.429; 0.858]$. Recently, Oguic et $al.$ (2013) validated their code based on fourth-order compact schemes in the inhomogeneous directions on the same reference data. Their results slightly improve those of Chung and Sung (2005) highlighting the importance of high-order schemes.

One will focus our attention here on the narrow gap case, which models quite faithfully flows in the rotor-stator gap of electrical motors. The aim of the present work is twofold : (i) providing some reference LES data and (ii) questioning the capabilities of a hybrid RANS / LES method, as well as the underlying RANS model, in predicting such flow.

2 Flow configuration and parameters

The cavity shown in Figure 1 may be characterized by two geometrical parameters : its aspect ratio $\Gamma = h/\Delta R = 10$ and its radius ratio $\eta = 8/9$. The inner cylinder is rotating at a constant rate Ω, while the outer one is stationary. An axial throughflow is imposed within the gap at a constant bulk velocity W_m. The main flow parameters are the rotational Reynolds number $Re_\Omega = \Omega R_1(R_2 - R_1)/\nu$ (in the range $[8.4 \times 10^3 - 2.5 \times 10^4]$) and the bulk Reynolds number $Re_Q = W_m(R_2 - R_1)/\nu$ ($= 3745$ or 5617), ν being the fluid kinematic viscosity. The results will be discussed in terms of the rotation parameter $N = Re_\Omega/Re_Q$, which will take four different values: $N = 1.49$, 2.98, 4.47 and 6.71.

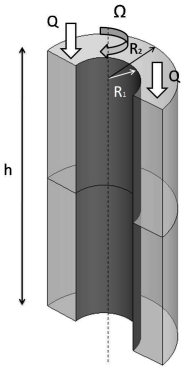

Figure 1: Sketch of the TCP system.

3 Numerical methods

The in-house code is based on semi-implicit and second-order accurate temporal schemes. The derivatives are approximated using fourth-order compact formula in the radial and axial directions and a Fourier

approximation in the tangential direction. The time splitting scheme is an improved projection method ensuring the incompressibility at each time step. The multidomain solver ensures the continuity of the solution and its first normal derivative across the conforming interface using an influence matrix technique (Abide and Viazzo, 2005). Periodic boundary conditions are applied in the axial and circumferential ($3\pi/4$ periodicity) directions and no-slip boundary conditions are imposed on the walls. The cavity has been decomposed into two subdomains in the axial direction. Two subgrid scale models will be tested in the following: a dynamic Smagorinsky model (denoted LES-SD) and the WALE model (LES-WALE). Two mesh grids containing ($N_r \times N_\theta \times N_z$)=($65 \times 144 \times 130$) and ($65 \times 144 \times 130$) points have been used for $N = 6.71$ and $N \leq 4.47$ respectively. The time step δt remains in the range $[3-8] \times 10^{-5}$ s. The present code has been fully validated by Oguic et $al.$ (2013) for $\eta = 0.5$.

The code used for RANS and hybrid RANS/LES simulations is the open-source *Code_Saturne*, developed by EDF (Archambeau et $al.$, 2004). It is a finite volume solver written in cartesian coordinates. A SIMPLEC algorithm, with the Rhie and Chow interpolation, is used for pressure-velocity coupling. Concerning hybrid RANS/LES calculations, convective fluxes are approximated by a second-order centered scheme for momentum and a first-order upwind scheme for subfilter quantities. Time marching uses a Crank-Nicholson second-order scheme. In RANS mode, convective fluxes are approximated by a first-order upwind scheme and a first-order time scheme. For both approaches, the elliptic blending Reynolds Stress Model of Manceau and Hanjalic (2005) is used. The hybrid method is the equivalent DES of Manceau et $al.$ (2010). The hybrid RANS/LES mesh contains 60^3 cells assuming a $\pi/2$-periodicity in the tangential direction and a periodic flow in the axial direction. The time step (normalized by $t_P = \Delta R/W_m$) is fixed to 1.4×10^{-2}. The RANS mesh is a 1D grid of 60 cells. No-slip boundary conditions are imposed on the walls.

4 Turbulence models

Various levels of modelling are presented. Emphasis is first put on the hybrid RANS/LES method. Afterwards, the subfilter closure and RANS model will be briefly presented, as well as the subgrid-scale models used for LES.

Hybrid method

The hybrid method used for the present work is the "Equivalent DES" of Manceau *et al.*(2010). This approach was first derived for the purpose of bridging the PITM (Partially Integrated Transport Model) of Chaouat & Schiestel (2005), and the DES (Detached Eddy Simulation) method. Indeed, the first is fully justified from a theoretical point of view, while the second one was developped on a rather phenomenological basis. First, the PITM was generalized by Fadai-Ghotbi *et al.*to inhomogeneous flows, considering temporal filtering, rather than spatial filtering. Indeed, inhomogeneous flows are more frequent. Since, in this kind of flow, the RANS operator corresponds, by ergodicity, to temporal averaging. Since any seamless (continuously transitioning) RANS/LES method must tend to RANS, at large filter width, inhomogeneous flow studies need then to consider hybrid RANS / temporal LES. Nevertheless, from a pragmatical point of view, considering RANS / TLES hybridization does not cause any difficulty in implementing models or special terms, since Fadai-Ghotbi *et al.*showed that applying Temporal PITM (T-PITM) to a inhomogeneous stationary flow is just equivalent to applying PITM to homogeneous, statistically unsteady flow. Actually, one must just keep in mind that "hybrid RANS/LES" is to be understood in a general way, including temporal LES. The advantage of Detached Eddy Simulation lies in its simplicity and robustness. The idea of Manceau *et al.*(2010), was thus to derive an approach bridging it with T-PITM. This latter is, in spite of its theoretical justification, not very easy to implement in any code, showing some numerical issues. An equivalence criterion was then determined between T-PITM and DES, providing some theoretical justification to the latter, and allowing to interprete it as a hybrid RANS / temporal LES method. This equivalence criterion was derived analytically for equilibrium flows, but was successfully tested on a flow over a periodic hill, involving massive separation (Friess & Manceau, 2012).
The principle of DES is to magnify the dissipation term of the transport equation for either subfilter turbulent kinetic k_{SFS} energy or subfilter stresses $\tau_{ij\,SFS}$, damping the modelled energy and allowing large scale eddies to be resolved:

$$\varepsilon_{ij}^{DES} = \frac{k_{SFS}^{3/2}}{\varepsilon_{SFS} L} \varepsilon_{ij\,SFS} \,. \tag{1}$$

While classical DES uses the local grid step to determine the length scale L in (1), equivalent DES uses the ratio r defined as :

$$r = \frac{k_m}{k} \,, \tag{2}$$

where k is the total turbulent kinetic energy, and k_m its counterpart contained in the modelled (subfilter) scales. At the RANS limit, r tends to 1, and at the DNS limit, it tends to 0. The advantage of r is that it can be estimated using a spatial or a temporal energy spectrum. As shown by Friess & Manceau (2012), r can be evaluated as :

$$\begin{aligned} r &= \frac{1}{k} \int_{\omega_c}^{\infty} E_T(\omega)\, d\omega \\ &= \min\left(1, \frac{1}{\beta_0} \left(\frac{U_s}{\sqrt{k}}\right)^{2/3} \left(\omega_c \frac{k}{\varepsilon}\right)^{-2/3}\right). \end{aligned} \tag{3}$$

β_0 being a constant derived from the Kolmogorov constant (we used 0.3 here), U_S a sweeping velocity and ω_c the cutoff frequency of the considered filter. It can be defined as :

$$\omega_c = \min\left(\frac{\pi}{\mathrm{dt}}; \frac{U_s \pi}{\Delta}\right) , \qquad (4)$$

where dt and Δ are the time and grid steps, respectively. Finally, following Manceau *et al.*(2010), the length scale L entering (1) is :

$$L = \frac{r^{3/2}}{1 + \frac{C_{\varepsilon 2} - C_{\varepsilon 1}}{C_{\varepsilon 1}}(1 - r^{C_{\varepsilon 1}/C_{\varepsilon 2}})} \frac{k^{3/2}}{\varepsilon} , \qquad (5)$$

RANS model and subfilter closure

In the temporally-filtered Navier-Stokes equation, the subfilter stresses must be modeled such a way that, making the temporal filter width go to infinity, the equations tend to the RANS equations. In particular, one of the main objectives of hybrid methods is to use RANS closures in the near-wall regions, to avoid the very fine resolution required by LES. In that aim, the RANS model proposed by Manceau & Hanjalić (2002), the so-called *elliptic blending Reynolds-Stress Model* (EB-RSM), is adapted to the hybrid temporal LES context. In this model, an elliptic relaxation equation is solved for a scalar α :

$$\alpha - L_{SFS}^2 \nabla^2 \alpha = 1 , \qquad (6)$$

which is a sensor of the distance to the wall ($\alpha = 0$ at the wall, and 1 far away), and is used to blend near-wall and homogeneous formulations for the redistribution and dissipation terms of the transport equations for subfilter stresses (see Fadai-Ghotbi *et al.*, 2010, for details) :

$$\phi^*_{ij} - \varepsilon_{ij} = \alpha^3 (\phi^*_{ij} - \varepsilon_{ij})_{\text{wall}} + (1 - \alpha^3)(\phi^*_{ij} - \varepsilon_{ij})_{\text{homogeneous}} . \qquad (7)$$

Under its RANS form, EB-RSM was successfully applied to several flows, such as non-rotating and rotating channels, impinging jets or mixed and natural convection flows. It was recently adapted by Fadai-Ghotbi *et al.*. (2010) to serve as a subfilter-stress model in the framework of T-PITM. In the present work, it is also applied as a model for the equivalent DES, by simply substituting the dissipation in the fashion of Eq. (1) in the Reynolds-stress transport equations.

Subgrid-scale model

Eventually, LES calculations were performed using the Wall-Adapting Local Eddy Viscosity (WALE) model of Nicoud & Ducros (1999). This choice was motivated by a better numerical stability than the dynamic Smagorinsky model, and its quality in near-wall treatment without damping functions. The subgrid viscosity is given by :

$$\nu_t = (C_w \Delta)^2 \frac{(S^d_{ij} S^d_{ij})^{3/2}}{(\overline{S}_{ij}\overline{S}_{ij})^{5/2} + (S^d_{ij} S^d_{ij})^{5/4}} , \qquad (8)$$

where C_w is a constant, Δ the grid step, $\overline{S}_{ij}$ the filtered strain-rate tensor, and S^d_{ij} the deviatoric part of the squared filtered velocity gradient tensor.

5 Results

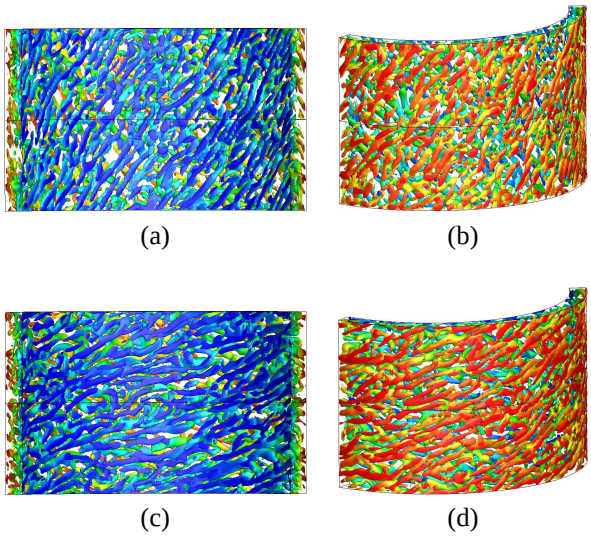

Figure 2: Iso-values of the Q criterion along the rotor (a,c) and along the stator (b,d) obtained by LES-WALE for: $N = 1.49$ (a,b); $N = 6.71$ (c,d).

Figure 2 presents the iso-values of the Q criterion obtained by LES-WALE for the two extrema values of the rotation parameter N. It highlights the presence of 3D unsteady coherent structures within the two boundary layers. They appear as thin negative spiral patterns along the rotor as they roll up in the opposite sense of the inner cylinder rotation. They are very similar to those obtained in a middle gap cavity by Oguic et $al.$ (2013). The same spiral network is obtained along the stator with a positive angle. For $N = 1.49$, these structures are more aligned with the axial direction as the effect of the axial flow is comparable to the one of rotation ($N \simeq 1$). They get progressively inclined with the tangential direction when the rotation rate (or N) increases. As examples, along the rotor, the angle formed by the spirals with the tangential direction is equal to $45°$ for $N = 1.49$ and to $16°$ for $N = 6.71$. From a numerical point of view, there is no evidence of structures at the interface between the two subdomains produced by a numerical artifact, which valids the multidomain approach. These structures may play a key role in the wall heat transfer process. They could explain why most of the RANS models, which assume the base flow as being stationary and axisymmetric, fail to predict the right distributions of the heat transfer coefficient.

Figure 3 presents the iso-values of the Q criterion, obtained by the hybrid RANS/LES approach, for the two highest values of the rotation parameter N. Due to the use of a coarser mesh, only the rotor side is

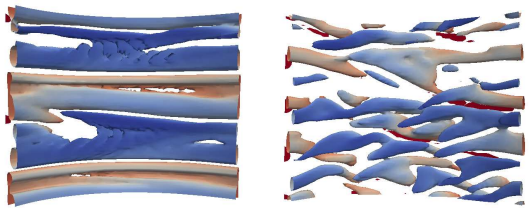

$N = 4.47$ $N = 6.71$

Figure 3: Iso-values of the Q criterion, colored by the radial coordinate r, obtained by hybrid RANS/LES, for $N = 4.47$ and 6.71.

shown, contrary to LES results. Despite the structure density is lower than for LES, net-shaped streaks are captured, with angles very similar to the ones given by LES. It is noticeable that some streaks are also obtained within the boundary layers, but this approach is unable to capture so well the thin coherent structures, unlike LES. The reason why $N = 1.49$ is not shown for hybrid RANS/LES, is that the calculation ended up to a RANS level, thus without capturing a ny coherent structures.

Figures 4 through 9 show a comparison between LES, RANS and hybrid RANS/LES statistics of the flow, for each value of the rotation parameter N. Hereafter, the LES results will be commented first, then the RANS results. Eventually, the hybrid RANS/LES will be paid more attention to.

The two LES provide the same mean velocity

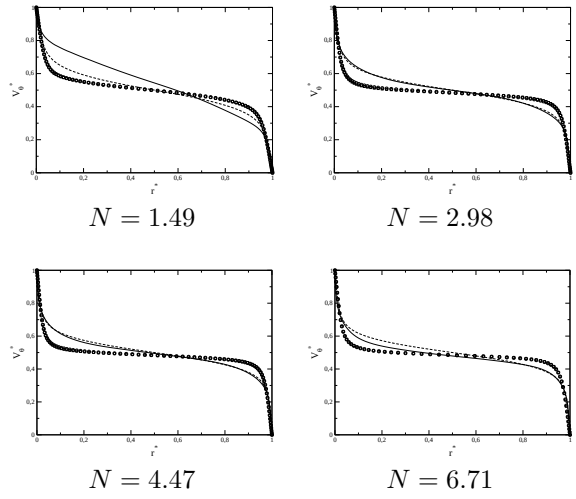

$N = 1.49$ $N = 2.98$

$N = 4.47$ $N = 6.71$

Figure 4: Radial distribution of the mean tangential $V_\theta^* = V_\theta/(\Omega R_1)$ velocity component for all four cases ; Comparisons between the LES-WALE (squares), the LES-SD (circles), RANS (dashed lines) and hybrid RANS/LES (solid lines).

profiles (Fig.4). The azimuthal velocity profiles, normalized by the rotor's speed, $V_\theta^* = V_\theta/(\Omega R_1)$ vary very weakly with the rotation parameter N such that $V_\theta^* = 0.5$ at mid-gap. One can just notice that, at low

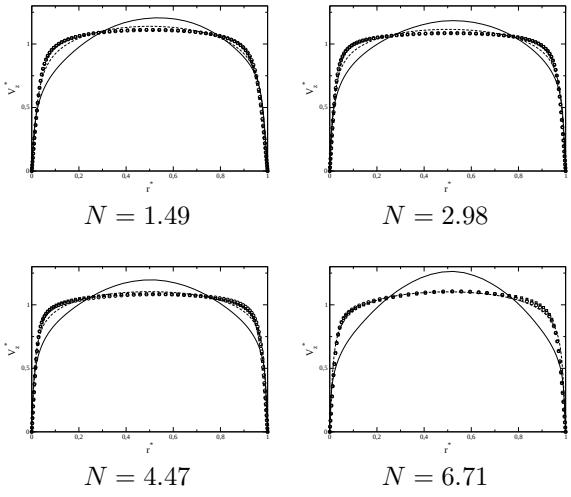

$N = 1.49$ $N = 2.98$

$N = 4.47$ $N = 6.71$

Figure 5: Radial distribution of the axial $V_z^* = V_z/W_m$ velocity component. Same legend as Figure 4.

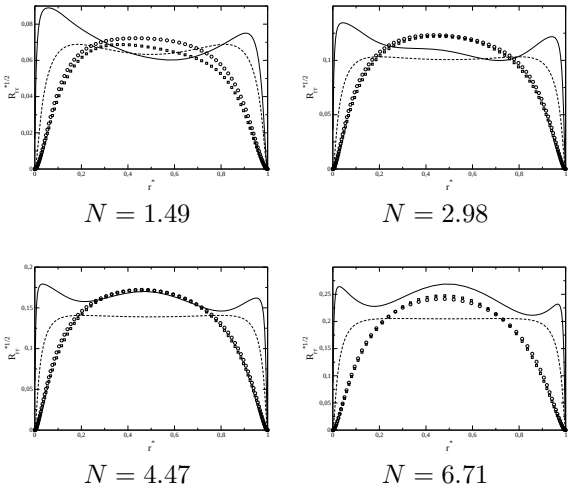

$N = 1.49$ $N = 2.98$

$N = 4.47$ $N = 6.71$

Figure 6: Radial distribution of the root-mean square Reynolds stress tensor component $R_{rr}^{1/2*} = \sqrt{\overline{v_r'^2}}/W_m$. Same legend as Figure 4.

N values, V_θ^* varies with $1/r$ in the gap and gets constant at high N. In that case, the profile resembles the Batchelor profile obtained in unmerged boundary layer interdisk flows. The axial velocity profiles is close to the turbulent Poiseuille profiles encountered in pipe flows and do not vary with N. Regarding the distributions of the two Reynolds stress tensor components, turbulence is mainly concentrated along the walls where remarkably high turbulence intensity peaks are observed. The LES-WALE may be considered as the reference data as it has been fully validated by Oguic et $al.$ (2013) for $\eta = 0.5$. The LES-SD provides here very similar results. It slightly overestimates the $R_{\theta\theta}$ component within the gap at $N = 6.71$. The LES-WALE is moreover less time consuming as

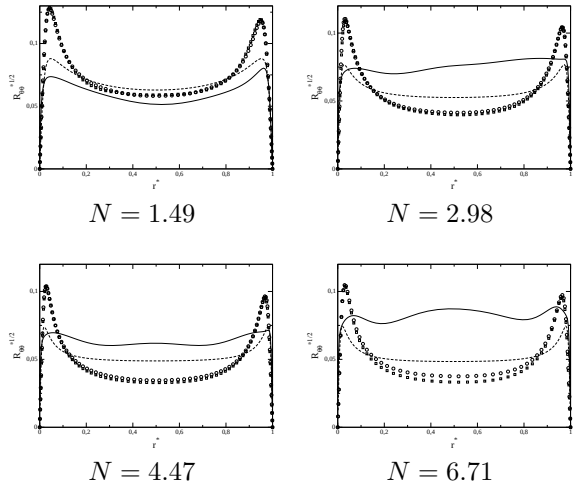

Figure 7: Radial distribution of the root-mean square Reynolds stress tensor component $R_{\theta\theta}^{1/2*} = \sqrt{\overline{v_\theta'^2}}/(\Omega R_1)$. Same legend as Figure 4.

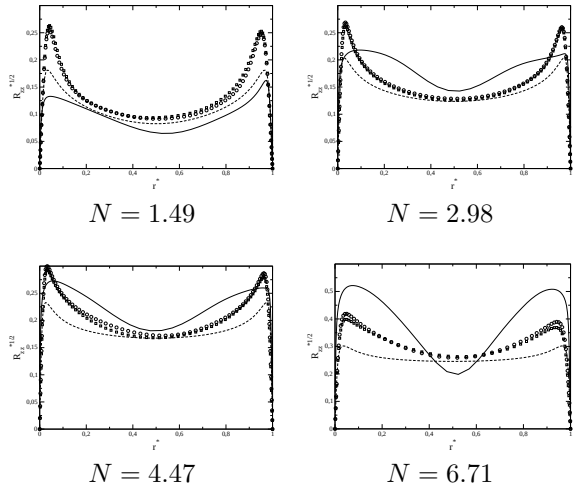

Figure 8: Radial distribution of the root-mean square Reynolds stress tensor component $R_{zz}^{1/2*} = \sqrt{\overline{v_z'^2}}/W_m$. Same legend as Figure 4.

the time per iteration is 16.09 s for $N = 6.71$ to be compared to 18.53 s for the LES-SD, with similar wall coordinates.

The RANS model predicts reasonably the statistics of the flow, though the normalized tangential velocity profiles V_θ^* seem quite insensitive to the value of N. However, the near-wall peaks predicted by the reference LES, for most of Reynolds stresses, are rather well captured by the EB-RSM model, especially their radial location. The asymmetry of the aforementionned peaks, is not well reproduced by EB-RSM, but this may be due to numerics, rather than the model itself. A further study is needed, on that point. Eventuially, those quite satisfactory results may be linked

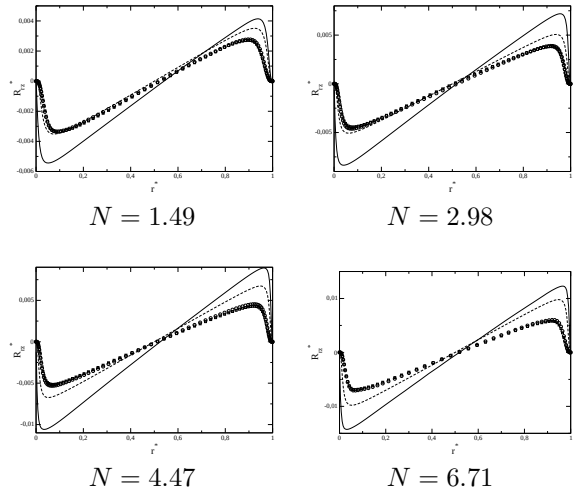

Figure 9: Radial distribution of the Reynolds stress tensor component $R_{rz}^* = \overline{v_r' v_z'}/W_m^2$. Same legend as Figure 4.

to the fact that the EB-RSM model is supposed to be well suited for wall-bounded flows involving attached boundary layers and exhibiting three-dimensional features.

The hybrid RANS/LES approach's success is mixed, with a significant dependance, not only on N, but also on the effective Reynolds number Re_{eff}. This latter is based on the effective velocity $V_{\text{eff}} = \sqrt{W_m^2 + 0.5\,(\Omega R_1)^2}$, which is a rough estimate of the resulting bulk velocity, in the plane tangential to the walls.

Table 1 summarizes the values of the three Reynolds numbers : axial, rotational and effective, Reynolds numbers. It is important to note that, despite 6.71 is the highest value for N, this case has the lowest axial Reynolds number, which is 3745. This value is rather low. Recalling that hybrid RANS/LES methods are rather designed for predicting high-Reynolds flows, one can explain why the case $N = 1.49$, having the lowest effective Reynolds number, the hybrid RANS/LES approach exhibits a bad overall prediction quality, for the flow statistics. Concerning other cases, the prediction quality of the hybrid RANS/LES approach is more contrasted.

Indeed, a low value of the axial Reynolds number Re_Q (case $N = 6.71$) leads to a quite bad description of statistics involving the axial component z. Similarly, a low value of the rotational Reynolds number Re_Ω results in a particularly poor prediction of statistics involving the azimuthal component θ. Reciprocally, more satisfactory results are obtained for higher Reynolds values : e.g. the peaks of ${R_{zz}^*}^{1/2}$ are better described by the hybrid approach, than by RANS, for cases $N = 2.98$ and $N = 4.47$. Similarly, there is a real gain in the prediction of V_θ^* and ${R_{\theta\theta}^*}^{1/2}$, for cases $N = 4.47$ and $N = 6.71$. The prediction of ${R_{rr}^*}^{1/2}$

seems rather sensitive to the effective Reynolds number Re_{eff}.
It is worth mentioning that the overstimation of Reynolds stress components is certainly due to the value of the constant β_0 entering Eq (3).
Eventually, one can guess there are thresholds for those Reynolds numbers. Below those thresholds, the hybrid RANS/LES approach does not improve the prediction of the flow statistics, in comparison with RANS. Above those thresholds, significant bettering is observed. Concerning Re_Q, the value of 5617 seems above, and 3745 unsufficient, whereas, for Re_Ω, 16755 seems above the threshold, and 8378 below it.

N	1.49	2.98	4.47	6.71
Re_Q		5617		3745
Re_Ω	8378	16755	25133	
Re_{eff}	8164	13112	18368	18162

Table 1: Values of axial, rotational and effective Reynolds numbers, for all four cases.

6 Conclusions

The present work is a step forward in the modeling of turbulent Taylor-Couette-Poiseuille flows in a narrow gap cavity. Four values of the rotation parameter N have been considered in the framework of a benchmark including two LES implemented in an in-house code and RANS and hybrid RANS/LES approach implemented in *Code_Saturne*. Assuming that Large Eddy Simulation results can be considered as reference data (Oguic et $al.$, 2013), the hybrid RANS/LES approach does not really improve the predictions of the RANS model for both the mean and turbulent fields, especially for the cases with lower values of the Reynolds number Re_{eff} based on the effective velocity. This tendency has already been observed by Fadai-Ghotbi et $al.$ (2010) for turbulent channel flows at moderate Reynolds numbers. The LES models highlight the presence of 3D coherent structures along both walls, appearing as two spiral networks whose angles strongly vary with N. In spite of the contrasted results of the hybrid RANS/LES approach on the statistics of the flow, instantaneous fields show similar features as LES, especially net-shaped streaks with acceptable angles.

Acknowledgments

This work was financially supported by Liebherr Aerospace (project “Entrefer moteur”) and by the LABEX MEC (ANR-11-LABX-0092).

References

Abide, S. and Viazzo, S. (2005), A 2D compact fourth-order projection decomposition method, *J. Comp. Phys.*, Vol. 206, pp. 252-276.

Archambeau, F., Méchitoua, N. and Sakiz, M. (2004), Code Saturne: a finite volume code for the computation of turbulent incompressible flows - Industrial applications, *Int. J. Finite Volume*, ISSN1634 (0655).

Chaouat, B. and Schiestel, R. (2005), A new partially integrated transport model for subgrid-scale stresses and dissipation rate for turbulent developing flows, *Phys. Fluids*, Vol. 17, 065106.

Chung, S. Y. and Sung, H. J. (2005), Large-eddy simulation of turbulent flow in a concentric annulus with rotation of an inner cylinder, *Int. J. Heat Fluid Flow*, Vol. 26, pp. 191-203.

Escudier, M. P. and Gouldson, I. W. (1995), Concentric annular flow with centerbody rotation of a Newtonian and a shear-thinning liquid, *Int. J. Heat and Fluid Flow*, Vol. 16, pp. 156-162.

Fadai-Ghotbi, A., Friess, C., Manceau, R. and Borée, J. (2010), A seamless hybrid RANS/LES model based on transport equations for the subgrid stresses and elliptic blending, *Phys. Fluids*, Vol. 22, 055104.

Fadai-Ghotbi, A., Friess, C., Manceau, R., Gatski, T.B. and Borée, J. (2010), Temporal filtering : a consistent formalism for seamless hybrid RANS/LES in inhomogeneous turbulence, *Int. J. Heat Fluid Flow*, Vol. 31, pp.378-389.

Friess, C. and Manceau, R. (2012), Investigation of the equivalence of two hybrid temporal-LES methods based on elliptic blending in separated flows, *Proc. 7th Int. Symp. Turbulence, Heat and Mass Transfer*, Palermo.

Kaye, J. and Elgar, E. C. (1958), Modes of Adiabatic and Diabatic Fluid Flow in an Annulus With an Inner Rotating Cylinder, *Trans. ASME*, Vol. 80, pp. 753-765.

Kuosa, M., Sallinen, P. and Larjola, J. (2004), Numerical and experimental modelling of gas flow and heat transfer in the air gap of an electric machine, *J. Thermal Science*, Vol. 13, pp. 264-278.

Manceau, R., Friess, C. and Gatski, T.B. (2010), Of the interpretation of DES as a hybrid RANS / temporal LES method, *8th ERCOFTAC Int. Symp. Eng. Turbulence Modelling Measurements*, Marseille.

Manceau, R., Gatski, T.B. and Friess, C. (2010), Recent progress in Temporal-LES/RANS modeling, *Proc. Vth Eur. Conf. Comput. Fluid Dyn.*, Lisbon.

Manceau, R. and Hanjalic, K. (2002), Elliptic blending model: a new near-wall Reynolds-stress turbulence closure, *Phys. Fluids*, Vol. 14(2), pp. 744-754.

Naser, J. A. (1997), Prediction of Newtonian and Non-Newtonian flow through concentric annulus with centerbody rotation, *Int. Conf. on CFS in Mineral and Metal Processing and Power Generation*, CSIRO.

Nicoud, F. and Ducros, F. (1999), Subgrid-Scale Stress Modelling Based on the Square of the Velocity Gradient Tensor, *Flow, Turb. & Comb.*, Vol.62, pp. 183-200.

Nouri, J. M. and Whitelaw, J. H. (1994), Flow of Newtonian and Non-Newtonian Fluids in a Concentric Annulus With Rotation of the Inner Cylinder, *J. Fluid Eng.*, Vol. 116, pp. 821-827.

Oguic, R., Poncet, S. and Viazzo, S. (2013), Numerical simulations of a middle gap turbulent Taylor-Couette-Poiseuille flow, *DLES 9*, Dresden.